Utilisation of Extended Slow Heating (ESH) pyrolysis and core analysis for determination of oil saturations and porosity correction.

Wael F. Al-Masri[1, *], *Bettina* Jenei[3], *Arka* Rudra[2], *Hamed* Sanei[2], *and Henrik I.* Petersen[1]

[1] Geological Survey of Denmark and Greenland, Department of Geo-energy and Storage, 1350 Copenhagen K, Denmark
[2] Aarhus University, Department of Geoscience, 8000 Aarhus C, Denmark
[3] Clausthal University of Technology, Institute of Subsurface Energy Systems, 38678 Clausthal-Zellerfeld, Germany

Abstract. Extended Slow Heating (ESH) pyrolysis is applied to assess oil fractions in reservoir rocks. It offers a novel approach to estimate oil saturation, as presented by a case study from the Nini West oilfield (Danish North Sea). This method enables cost-effective saturation estimation from minimal sample sizes, using cleaned core plugs to evaluate cleaning efficiency and adjust for porosity underestimation due to incomplete cleaning. ESH involves gradual pyrolysis of 50 mg dry, ground samples (100–650 °C at 10 °C/min) using a HAWK Pyrolysis and TOC analyser calibrated against oils with known gravity and API standards. Hydrocarbon release is continuously measured during pyrolysis, and oil fractions were defined based on their densities. ESH-derived oil saturation and API values aligned with direct measurements, confirming the method's reliability. Saturation values in $scCO_2$-flooded plugs were significantly lower, suggesting that lighter hydrocarbons were removed, leaving heavier, immobile fractions (solid bitumen/asphaltenes), although with minor quantities. The study, combining ESH, chromatography, porosity measurements, and cleaning techniques, reveals that solid bitumen and asphaltenes remain post-$scCO_2$ flooding and cleaning. ESH is a rapid and effective method for determining oil composition, saturation, and API gravity. Its low sample requirement allows for spatial oil composition analysis from cuttings, offering advantages over traditional core analysis methods.

1 Introduction

Crude oil varies in physical and chemical properties due to differences in the quantity of nonidentical hydrocarbon fractions having different sizes and compositions [1]. Efficiency of crude oil extraction is both dependent on crude oil composition and reservoir properties, lithology, porosity and permeability. One of the techniques that has been used to enhance oil recovery (EOR) is the injection of supercritical CO_2 ($scCO_2$). Triggered by the global climate change, geological carbon capture and storage (CCS) has emerged as a cornerstone strategy in mitigating rising atmospheric CO_2 levels [2,3]. Among the various CCS technologies, subsurface CO_2 injection – especially into depleted oil and gas reservoirs – offers a highly practical and technically feasible approach due to existing infrastructure and well-characterised geologic frameworks [4].

However, $scCO_2$ injection into hydrocarbon-bearing reservoirs brings a dual effect: it supports CO_2 sequestration while also mobilising remaining hydrocarbons. In EOR applications, $scCO_2$ dissolves into the remaining oil, reducing viscosity and improving flow properties [5–7]. Simultaneously, $scCO_2$ selectively extracts lighter hydrocarbon fractions – such as the diesel-range nC_{11}–nC_{21} components – while leaving behind heavier, viscous oil fractions with lower API gravity [8–10]. These residual heavy fractions, including asphaltenes and solid bitumen, may accumulate within pore networks and cause clogging, posing risks to injectivity and long-term CO_2 storage capacity [11–15].

In a CO_2 storage context, it is therefore important to have an understanding of the saturation and composition (oil fractions) of the remaining oil in the reservoir considered for CO_2 storage. Recently, the impact of $scCO_2$ injection on oil composition has been explored for depleted sandstone and chalk oil reservoirs in the Danish North Sea [13,14]. These studies employed a combination of ESH pyrolysis, gas chromatography, organic petrography, and porosity measurements to investigate the remaining oil composition. The mobility of the hydrocarbons was examined by $scCO_2$ flooding experiments conducted under reservoir conditions.

ESH pyrolysis, introduced by Sanei et al., provides a refined thermal program that enhances the resolution of oil fractions during slow ramp heating [16,17]. Its ability to quantify oil fractions from small sample sizes (e.g., 50 mg of ground rock) makes it a cost-effective tool for both

* Corresponding author: wfa@geus.dk

core and cuttings analysis. The ESH method, comparable to the modified Rock-Eval protocol proposed by Jones and Tobey [18], has gained wide application in evaluating reservoir quality and hydrocarbon composition for various purposes, including hydrocarbon-stained core and cuttings in conventional systems [19], hydrocarbon retention and recovery potential in shale mudstones [20–24], indicator of complete removal of hydrocarbons during shale cleaning [25,26], and hydrocarbon composition in depleted oil fields considered for CO_2 storage [13–15]. In the latter studies, ESH pyrolysis proved to be particularly valuable in assessing the spatial distribution, composition, and API gravity of the remaining oil before $scCO_2$ injection, and the change in oil composition after $scCO_2$ injection [13-15]. In the context of $scCO_2$ flooding, the ESH method was also used to assess the cleaning efficiency of core plugs used for restoration to original oil and brine conditions before flooding [14].

The ESH method gives the oil fractions in volume% (vol.%) while reservoir engineers work with oil saturations (%). In order to bridge this gap between petroleum geochemistry and petroleum engineering, this study presents a method to convert vol.% data derived from ESH pyrolysis into saturation%. The method is demonstrated by using the ESH data from the depleted Nini West oil field in the Danish North Sea presented by Petersen et al. [14] as a case study. Due to the small sample amount required and the short analysis time, this innovative method allows for an estimation of oil saturation in not only a few core plugs but also large quantities of cuttings samples. In addition, the saturation estimates of the cleaned core plugs are used to quantitatively evaluate cleaning efficiency and factor in adjustments for the porosity underestimation due to incomplete cleaning. This strategy outperforms traditional core plug analysis, which requires core plugging, extensive solvent extraction, and oil analysis.

2 Methods

2.1 Extended Slow Heating (ESH)

The ESH pyrolysis method represents an advanced thermal analysis technique tailored to investigate the distribution and composition of hydrocarbons in geological materials. Initially introduced by Sanei et al. and later adopted in studies such as those by Kurz et al. and Hawthorne et al., Steshøj et al., and Petersen et al., ESH modifies the conventional heating protocol by applying a reduced temperature ramp. [13–17,24,27]. This adjustment enhances the separation and resolution of different hydrocarbon fractions released from the rock matrix.

Unlike traditional pyrolysis approaches, which often employ rapid heating and risk underestimating heavier hydrocarbons in the S1 peak, ESH uses a gradual temperature increase, from 100 °C to 650 °C at a steady rate of 10 °C per minute, executed on a HAWK Pyrolysis and Total Organic Carbon (TOC) analyser (Wildcat Technologies). The slower ramp rate enables more efficient volatilisation of heavier molecules, which might otherwise be delayed or co-eluted with kerogen, appearing as a shoulder or broadening of the S2 peak. In this way, ESH delivers a more detailed and accurate hydrocarbon release profile see Fig. 1.

During the heating process, hydrocarbon evolution is continuously monitored using a Flame Ionisation Detector (FID), resulting in a high-resolution pyrogram. This curve is analysed using the ESH Slice&Dice algorithm, which divides the temperature spectrum into distinct intervals [13,15]. Each interval corresponds to hydrocarbons of increasing molecular size and density, with release temperature serving as a proxy for molecular weight and compositional complexity.

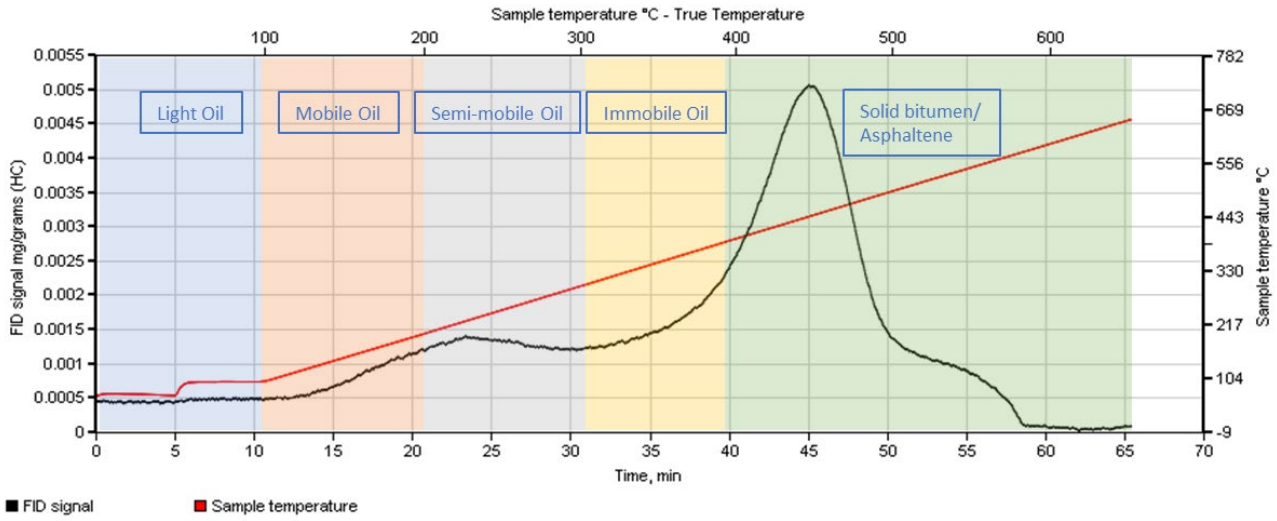

Fig. 1 Example of an ESH pyrogram from a CO_2-flooded core sample, illustrating the five temperature intervals defined by the Slice&Dice algorithm. The corresponding hydrocarbon fractions—light oil, mobile oil, semi-mobile oil, immobile oil, and solid bitumen/asphaltenes—are identified based on their volatilisation temperatures. The black curve represents the FID signal (hydrocarbon release), while the red line indicates the programmed sample temperature.

Based on calibrated density values, the method categorises hydrocarbons into five distinct fractions: light oil (0–100 °C; 0.773 g/cm³), movable oil (100–200 °C; 0.807 g/cm³), semi-movable oil (200–300 °C; 0.899 g/cm³), non-movable oil (300–375 °C; 1.022 g/cm³), and solid bitumen or asphaltenes (375–650 °C; 1.2 g/cm³). These classes are derived from the pyrolysis behaviour of reference compounds and help interpret the types of hydrocarbons present in the sample.

Quantitative assessment of each hydrocarbon fraction is achieved by calibrating the FID response using known standards. To ensure the highest accuracy, the HAWK system is calibrated using Whole rock Type standard (WT2), with acquisition parameters maintained within a 5% error margin. A procedural blank is run prior to each analysis to monitor and correct for background signals. The method estimates hydrocarbon concentrations in weight per cent (wt.%), which are then converted to volume per cent (vol.%) by accounting for the specific density of each fraction and the sample's initial mass. This transformation enables the volumetric estimation of hydrocarbons per unit volume of rock.

It is important to recognise that while the classification system offers detailed compositional data, it is based on pure compounds and does not fully capture the complex phase behaviour seen in actual reservoir fluids, where different hydrocarbon types often coexist with overlapping physical properties. As such, direct application to reservoir flow predictions requires caution.

In addition to hydrocarbon profiling, the ESH technique can detect chemical signatures such as carbonyl (C=O) groups, indicative of oxygen-rich or heavily altered organic matter, including asphaltenes and polar compounds. These insights provide additional information on the chemical nature of the immobile oil fractions.

One notable application of ESH is in assessing the effectiveness of core cleaning procedures. When applied to samples presumed clean, ESH can reveal residual hydrocarbons that may occupy pore space and hinder helium penetration during porosity analysis via He-porosimetry. Such residuals can lead to underestimations of effective porosity. Accordingly, ESH offers a method to correct porosity measurements by accounting for these retained hydrocarbons, thereby enhancing the reliability of petrophysical data [28–30].

Following this methodological overview, a derivation is provided for calculating oil saturation from ESH-based volume estimates. Additionally, a correction formula is introduced to refine He-porosimetry-derived porosity values by compensating for hydrocarbon volumes still present in cleaned samples, contributing to more accurate subsurface characterisation.

2.2 Saturation Estimate and Porosity Correction

The ESH pyrolysis yields the distribution of hydrocarbon fractions as volume per cent (vol.%), relative to the rock-hydrocarbon system's total dry mass or volume, with water and gas content deliberately excluded. Which reads:

$$Vol.\%\,(i) = \frac{V_i}{V_R + \sum_{i=1}^{n} V_i} 100\% \qquad (1)$$

In this framework, the volume V has the dimension of $[L^3]$, and the subscript R refers to rock, while i denotes the i-th hydrocarbon species—specifically: light oil, movable oil, semi-movable oil, non-movable oil, and solid bitumen/asphaltenes. This volumetric data can be interpreted as follows: for every 100 ml of bulk sample (rock plus hydrocarbons), $(Vol.\%(i))$ corresponds to the volume in millilitres of hydrocarbon fraction i, and the remaining $(100 - \sum_{i=1}^{n} V_i)$ ml represents the volume of rock matrix. In contrast, saturation (S_i) is the term that defines the proportion of the pore volume occupied by the hydrocarbon species i. To determine this, the porosity (ϕ) of the rock must be known. Porosity is defined as the ratio of the pore volume (V_p) to the total volume of the sample (i.e., $V_p + V_R$), where V_R is the rock grain volume. From this definition, it is possible to derive the pore volume associated with a given rock volume, and consequently, the saturation (Si) of each hydrocarbon fraction:

$$S_i = \frac{Vol.\%(i)}{\frac{\phi}{1-\phi}\left(100 - \sum_{i=1}^{n} Vol.\%\,(i)\right)}\ 100\% \qquad (2)$$

In routine core analysis workflows, helium porosimetry is the industry-accepted method for measuring effective porosity. This technique assumes that all fluids have been completely removed from the pore network, as helium is used to probe the available pore space by expanding from a reference volume to the pore volume. However, if hydrocarbons are only partially removed, as is often the case, some pore volume remains occupied by residual hydrocarbons. This leads to underestimating the true pore volume and, by extension, the porosity. The retained hydrocarbons artificially increase the rock volume, causing helium gas to expand into a reduced pore space. Therefore, the measured porosity (ϕ_m) from helium porosimetry is less than the actual porosity (ϕ). The discrepancy can be corrected by introducing a porosity correction factor, compensating for the remaining hydrocarbon volume in the cleaned core sample. Thus, the measured porosity, ϕ_m, measured by the He-porosimeter, can be expressed as:

$$\phi_m = \frac{V_p - V_{HC}}{V_T} = 1 - \frac{V_R + V_{HC}}{V_T} = \phi - \frac{V_{HC}}{V_T} \qquad (3)$$

The term $(-V_{HC}/V_T)$ is the correction factor needed to be added to the measured porosity. Conducting an ESH measurement on a cleaned sample gives the amount of hydrocarbon left in the core sample after cleaning. This value can be used to calculate the error in the porosity measurement and the correction factor as follows:

$$Vol.\%\,(HC) = \frac{V_{HC}}{V_R + V_{HC}} 100\% \qquad (4a)$$

where V_{HC} is equal to the sum of the hydrocarbon volume fraction, $\sum_{i=1}^{n} V_i$. Dividing both the nominator and the

denominator by the total volume, the previous equation reads:

$$Vol.\%\,(HC) = \frac{V_{HC}}{V_T}\frac{V_T}{V_R + V_{HC}}100\% \quad (4b)$$

Thus, the correction factor reads:

$$\frac{V_{HC}}{V_T} = Vol.\%\,(HC) * \frac{V_R + V_{HC}}{V_T}$$

$$\frac{V_{HC}}{V_T} = Vol.\%\,(HC) * (1 - \phi_m) \quad (5)$$

This correction factor not only improves the precision of porosity estimations but also serves as a quantitative metric for assessing the efficiency of solvent-based core cleaning procedures. Higher residual hydrocarbon volumes indicate incomplete cleaning, thereby guiding the selection of more effective cleaning strategies tailored to specific lithologies and reservoir conditions.

3 Case Study - The Nini West Storage Site

To demonstrate and validate the methodology for saturation estimation and porosity correction, we utilise ESH pyrolysis results from Petersen et al. [14]. The Nini West storage site, also known as "Project Greensand", was developed with the aim of injecting and permanently storing CO_2 in a depleted oil field in the Danish sector of the North Sea. The project was initiated in support of Denmark's ambitious targets to achieve a 70% reduction in greenhouse gas emissions by 2030 and net-zero emissions by 2050 [31,32]. The Nini West field is located in the Siri Canyon in the North Sea (Fig. 2), and contains a reservoir consisting of fine-grained glauconitic sandstones, securely sealed by a 900 m thick succession of mudstones (Horda and Lark Formations), providing a robust seal complex with high integrity [33–36].

In 2024, pilot injection of $scCO_2$ was successfully completed in the Nini West structure, and upon full implementation, the storage site is projected to achieve a storage capacity of up to 8 million tonnes of CO_2 per year. CO_2 is initially transported by ship to the offshore injection site, where it is injected into the reservoir at depths of 1700–1800 metres. As one of Europe's most mature offshore CCS ventures, Project Greensand serves as a strategic model for the repurposing of depleted hydrocarbon reservoirs, offering critical infrastructure solutions for regional and global climate goals across the North Sea [32].

In the following section, we first provide a brief overview of the geological characteristics of the Nini West Field. We then introduce the dataset employed in this study, expanding upon the sampling and analytical procedures described in Petersen et al [14]. This forms the basis for demonstrating the application and validation of the proposed saturation estimation and porosity correction methods.

3.1 Geological setting

The Nini West Field is located within the Siri Canyon of the Danish North Sea (Fig. 2a). The Siri Canyon itself, a major Palaeocene geological feature, trends east-northeast for approximately 120 kilometres from the eastern edge of the Danish Central Graben, extending across the Ringkøbing-Fyn High toward the Stavanger Platform (Fig. 2b).

The canyon system formed during the Palaeocene through deep incision of the Cretaceous–Danian Chalk Group. During Palaeocene and Miocene times, it was progressively infilled by hemipelagic and turbiditic marls and mudstones. Episodic deposition of sandy mass-flow and turbidite sediments during the Palaeocene–Eocene led to the accumulation of fine-grained, well-sorted glauconitic sandstones [33–35].

These sediments were transported via turbidite systems originating from the Stavanger Platform, and their deposition was closely linked to the backstepping of the Paleogene depositional systems. This resulted in the deposition of several sandstones embedded in the pelagic mudstones [33,34,37] (Fig. 2c). Owing to episodes of post-depositional remobilisation and fluidisation, the spatial arrangement of the sandstone bodies is notably intricate [33,38], resulting in reservoirs distributed across different stratigraphic horizons. Earlier deposited sandstones are capped by units within the Rogaland Group, while younger sandstones are sealed by extensive Eocene to Oligocene–Miocene marine mudstones of the Horda and Lark Formations (Fig. 2c).

The Nini West Field itself occupies a structural position on the western limb of the Nini anticline, a structure resulting from halokinetic movements associated with salt tectonism [39]. It forms part of a broader petroleum accumulation that is confined within a combination of structural and stratigraphic traps.

Sealing the reservoir is a thick succession—approximately 900 metres—of low-permeability mudstones from the Horda and Lark Formations, which provide an effective regional caprock system [34,36,40]. The reservoir is encountered at subsurface depths between 1700 and 1800 metres, where the prevailing formation temperature is around 60 °C. Petrographically, the reservoir is dominated by fine-grained, well-sorted sandstones in which quartz and glauconite are the major components, with glauconite content ranging between 20% and 30%. Minor mineral constituents include feldspars, micas, lithic fragments, and heavy minerals [35,38,41].

A distinguishing feature of the Nini West reservoir is its significant glauconite content. Detailed mineralogical investigations by Weibel et al. [42] revealed that glauconite grains predominantly exhibit a mixed-layer Fe-smectite/illite structure. Additionally, the sandstones host a variety of partially to fully glauconitised grains originating from different mineral precursors. Thin coatings of phyllosilicate cements, often developed on the surfaces of glauconite clasts, may exert a considerable influence on the reservoir's petrophysical properties, particularly permeability and mechanical behaviour. Importantly, the sands from this formation are markedly

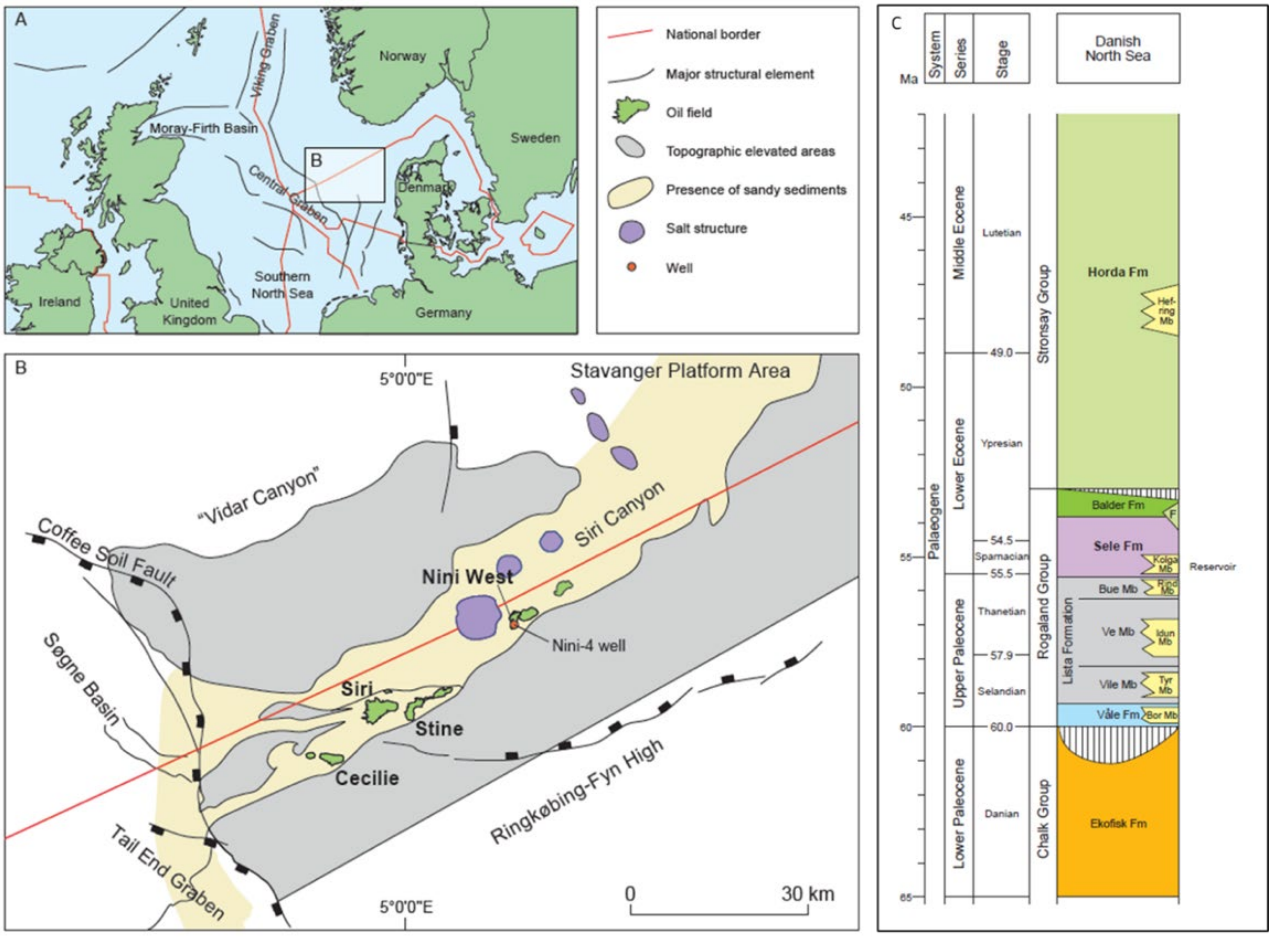

Fig. 2 A) Regional map illustrating the position of the Siri Canyon within the Danish sector of the North Sea; (B) Detailed location of the Nini-4 well within the Nini West reservoir of the Siri Canyon; (C) Stratigraphic column highlighting the Paleogene sandstone reservoir (Kolga Member) and the lower portion of the primary seal formed by the Eocene Horda Formation (Modified from [33,34,36]).

distinctive, with glauconitic clasts exhibiting anomalous behaviour during laboratory procedures. These grains tend to remain saturated with hydrocarbons and often retain oil even after extensive cleaning, posing a specific challenge in core preparation and petrophysical interpretation [14]. This unique behaviour underlines the need for careful assessment of cleaning efficiency, as investigated in the present study.

3.2 Data Set

This study employs a dataset of thirteen samples previously analysed using ESH pyrolysis as part of our previous study [14]. The samples originate from thirteen core plugs retrieved from the Nini-4 well within the Nini West Field, Siri Canyon, covering a depth interval between 1774.28 and 1782.67 meters. The collection encompasses preserved plugs, brine-stored preserved plugs, plugs cleaned by three different laboratory methods, a restored plug, and a restored plug subjected to supercritical CO_2 ($scCO_2$) flooding, summarised *in Table* 1. The conventional core analysis (CCAL) data—namely helium porosity, nitrogen gas permeability, and grain density—are available for most samples (GEUS in-house data and [43]), although interpolation from adjacent depths was necessary for two plugs, where direct measurements were unavailable. Overall, the plugs exhibit relatively uniform porosity values ranging from 35.00% to 35.83%, with a minor deviation observed at 33.80% (plug PB2), while grain densities span 2.690 to 2.716 g/cm³. Permeability values showed greater variability but remained favourable, ranging from approximately 1059 to 1249 mD.

The ESH pyrolysis program results are presented in Table 2 and incorporate the volumetric fraction composition of the saturating oil, as well as the estimated API of the oil. Note that the sum of the oil fractions does not equal the total oil volume fraction; this discrepancy is due to a minor hydrocarbon fraction bound to the matrix. For more information on the nuance of the method, work program and discussion on the ESH results, the reader is referred to [14]

3.3 Method validation and accuracy - Saturation calculation from ESH

The restored plug, REST1, was selected as a reference sample to validate oil saturation estimates obtained from ESH pyrolysis and assess the method's accuracy. A small

portion of material was first extracted from plug HSEC2 for ESH analysis, while the remaining REST1 sample underwent a complete restoration procedure.

During wettability restoration, REST1 was fully saturated with synthetic brine formulated to replicate the formation water chemistry. The plug was initially placed under vacuum for two hours to remove trapped gases, after which brine was introduced to achieve complete pore saturation. Full saturation was confirmed using the Archimedes method by submerging the plug in brine and measuring buoyancy.

The plug was then drained to a target connate water saturation (Swi = 30%) using the porous plate method. This involved placing the sample in a core holder fitted with a semi-permeable ceramic plate, using nitrogen (N_2) as the non-wetting phase. The ceramic plate had an 80 nm pore throat, favouring water wetting, and a theoretical N_2/water entry pressure of 35 bar. By applying a pore pressure of 13.8 barg, a saturation of 32.79% was achieved and later confirmed by gravimetric measurements (see Fig. 3).

Following drainage, N_2 was replaced with Stock Tank Oil (STO) under vacuum. Some brine evaporation occurred during this process, further reducing water saturation. The amount of water evaporated is adjusted by modifying the time under vacuum before introducing the STO. The STO, sourced from the Nini Field, underwent centrifugation to remove dissolved water and high-pressure filtration (7 μm) at room temperature to eliminate suspended solids.

The plug was then brought to reservoir pressure and temperature and aged for one month, followed by continued STO injection under the same conditions to fully restore reservoir wettability. Final fluid saturations of Sw = 30% and Soi = 70% were achieved and confirmed by comparing the weight of the sample after ageing to the dry conditions using a scale with an accuracy of ±0.01g, knowing the density of both fluids.

Table 1. Characterisation of the examined core samples*

Sample type	Sample name	Description	Depth	ϕ	k_{gas}	ρ_{grain}
			m (MD)	%	mD	g/cm^3
Preserved	PF1	Preserved plug	1775.78	35.11	1065	2.702
	PF2	Preserved plug	1775.97	35.00	1059	2.707
	PF3	Preserved plug	1776.90	35.05**	1325**	2.695**
	PB1	Preserved plug in brine	1774.28	35.73	813	2.707
	PB2	Preserved plug in brine	1777.27	33.80**	1080**	2.69**
	PB3	Preserved plug in brine	1782.67	35.23	769	2.699
Cleaned	DEC1	Diffusion-evaporation cleaning method	1776.88	35.39	1212	2.712
	CFC1	Cold flushing cleaning method	1776.85	35.46	1249	2.711
	CFC2	Cold flushing cleaning method	1776.88	35.39	1212	2.712
	HSEC1	Hot Soxhlet extraction cleaning method	1775.04	35.00	1180	2.690
	HSEC2	Hot Soxhlet extraction cleaning method	1776.11	35.50	fractured	2.700
Restored	REST1	Hot Soxhlet extraction, STO sat, aged 1 mth	1776.11	35.50	fractured	2.700
CO_2 flooded	CO2F1A	CO_2 flooded, STO sat., aged 1 mth, inlet A	1781.04	35.14	1122	2.716
	CO2F1B	CO_2 flooded, STO sat., aged 1 mth, inlet B	1781.04	35.14	1122	2.716

*Data from the GEUS Database and the CCAL report [43]

**Data not measured on plug but derived from the nearest plug

Table 2. Results of ESH analysis (adopted from [14])

Sample type	Sample name	Total oil	Light oil	Mobile oil	Semimobile oil	Immobile oil	Solid bitumen	ESH API
		vol.%	vol.%	vol.%	vol.%	vol.%	vol.%	°
Preserved	PF1	18.09	0.20	6.28	4.90	1.29	5.26	34
	PF2	16.16	0.17	6.38	4.33	0.99	4.14	36
	PF3	21.31	0.22	6.12	8.66	2.27	3.98	37
	PB1	11.57	0.07	3.91	2.95	0.68	3.8	33
	PB2	16.78	0.20	4.91	5.55	2.06	3.98	35
	PB3	9.15	0.02	1.72	2.04	0.63	4.56	27
Cleaned	DEC1	1.88	0	0.12	0.09	0	1.55	14
	CFC1	1.41	0	0	0	0	1.29	n.d.
	HSEC1	1.63	0	0	0	0	1.53	n.d.
	HSEC2	0.72	0	0	0	0	0.67	n.d.
Restored	REST1	28.39	0.52	9.20	10.01	2.56	5.88	37
CO_2 flooded	CO2F1A	2.02	0	0	0.01	0.08	1.86	n.d.
	CO2F1B	1.74	0	0	0	0.04	1.63	n.d.

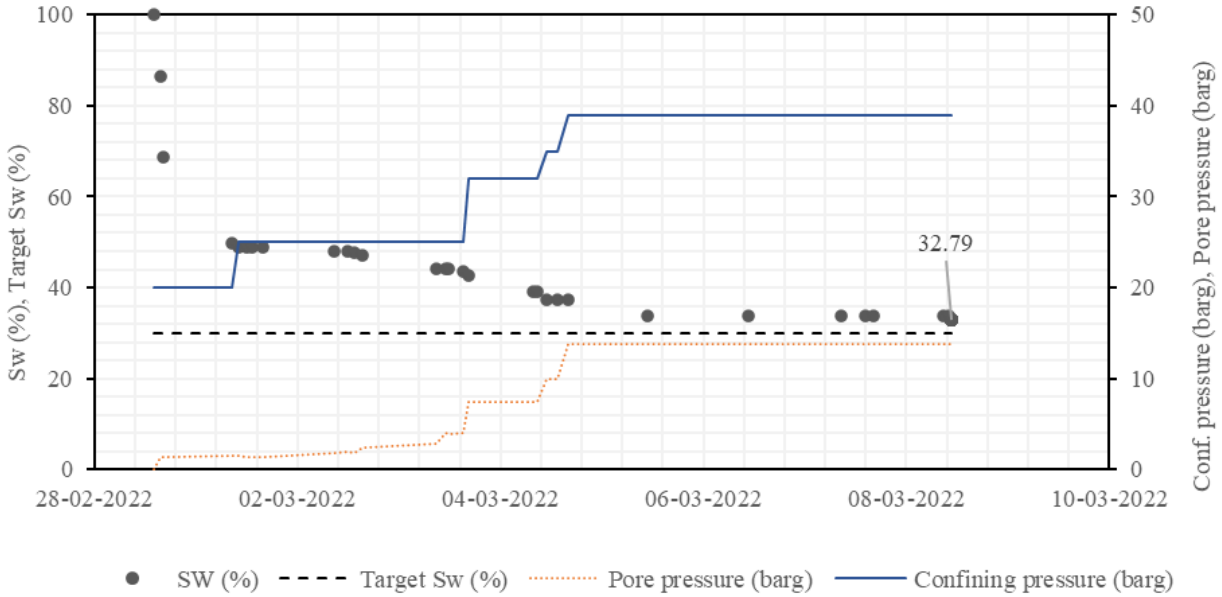

Fig. 3 Results of the porous plate drainage on the sample REST1, including: pore pressure (dotted line); target saturation (dashed line); confining pressure (solid line); and saturation (circles)

ESH analysis of REST1 yielded oil saturations of 70.7% (including matrix-bound hydrocarbons) and 70.2% (excluding them), both closely aligning with the gravimetrically measured saturation of 70%. A porosity correction of 0.43 porosity unit (PU) was applied before calculating the saturation, establishing REST1 as a robust benchmark for interpreting ESH results across the remaining sample set (See Table 3)

3.4 Porosity correction results

The results of the ESH show varying amounts of remaining hydrocarbons in the cleaned core plugs, depending on the cleaning method (ranging from 0.72 to 1.88 vol.%). None of the cleaning methods resulted in the complete removal of hydrocarbons (See Table 2). The porosity correction factor for each cleaned sample is calculated by applying the abovementioned procedure. The porosity underestimation ranges between 0.43 PU and 1.14 PU; see Table 4. However, the diffusion-evaporation method is considered unsuitable for cleaning the Nini-4 core plugs due to the presence of minor quantities of mobile and light hydrocarbons. The results from the cold-flushed plug CFC1 and the hot Soxhlet-extracted plug HSEC1 are almost identical, suggesting that cold flushing is the best method to clean the core samples since applying the hot Soxhlet extraction might compromise the integrity of the pore structure.

In the case of plug HSEC2, the hot Soxhlet extraction resulted in an impressive removal of the oil, in which only 1.3% of the pore volume was left uncleaned. This is equivalent to 0.43 PU porosity correction, which is half the porosity underestimation compared to the other cleaning methods. This might be a result of the smaller dimensions relative to the rest of the core plugs. Plug HSEC2 has a length of 1.5 cm, equivalent to 15.62 cc bulk volume, while the other plugs are from between 5 and 7cm, equivalent to between 54.64 and 76.49 cc bulk volume.

Table 3. Results ESH analysis converted to saturations

Sample type	Sample name	Total oil saturation (%)	Light oil saturation (%)	Mobile oil saturation (%)	Semimobile oil saturation (%)	Immobile oil saturation (%)	Solid bitumen saturation (%)
Preserved	PF1	39.4	0.4	13.7	10.7	2.8	11.5
	PF2	34.6	0.4	13.6	9.3	2.1	8.9
	PF3	48.5	0.5	13.9	19.7	5.2	9.1
	PB1	22.7	0.1	7.7	5.8	1.3	7.5
	PB2	38.1	0.5	11.2	12.6	4.7	9.0
	PB3	17.9	0	3.4	4.0	1.2	8.9
Cleaned	DEC1	3.3	0	0.2	0.2	0	2.8
	CFC1	2.5	0	0	0	0	2.3
	HSEC1	2.9	0	0	0	0	2.8
	HSEC2	1.3	0	0	0	0	1.2
Restored	REST1	70.7	1.3	22.9	24.9	6.4	14.7
CO_2 flooded	CO2F1A	3.7	0	0	0	0.2	3.4
	CO2F1B	3.2	0	0	0	0.1	3.0

Table 4. Measured porosity, porosity correction factor (VHC/VT), and corrected porosity of the cleaned samples

Sample name	Cleaning Method	ϕ %	VHC/VT PU	ϕ_{corr} %
DEC1	Evaporation	35.39	1.14	36.53
CFC1	Cold flushing	35.46	0.83	36.30
HSEC1	Soxhlet	35.00	0.99	35.99
HSEC2	Soxhlet	35.50	0.43	35.93

3.5 Summary of saturation estimates and comparison with other core samples

Following the implementation of suitable porosity corrections, an average value of 0.8 PU was used to adjust the porosity of both the preserved and CO_2-flooded samples. The correction factor for the remaining samples was determined individually, as direct measurements were obtained for each cleaned and restored sample. Refer to section 3.4 for details. The information in Table 2 was then converted into fluid saturations using the previously described methodology. The resulting values are presented in Table 3. A comparison of oil saturations between fresh-state plugs and those stored in brine revealed the following observation: the majority of light, mobile oil, and a notable portion of semi-mobile and immobile oil were displaced during storage. This displacement is attributed to gravity drainage and capillary forces acting over time. In contrast, solid hydrocarbon components, such as bitumen and asphaltenes, remained largely unaffected by the brine storage conditions.

An exception to this trend was observed in core plug PB2, where no evidence of oil mobilisation was detected. This anomalous result may be due to insufficient brine contact during storage, possibly caused by incomplete immersion, or the sample's location near the top of the core, where gravitational effects would be minimised.

Interestingly, the restored plug REST1 displayed higher levels of immobile oil and solid bitumen/asphaltenes compared to the preserved plugs, contrary to initial expectations. This increase is attributed to the ageing phase of the restoration process, during which a layer of heavy oil likely adhered to the surfaces of glauconite grains, modifying their surface wettability. Even after flushing the plug with fresh Stock Tank Oil (STO), this adhered heavy oil layer was not displaced, leading to an elevated immobile oil fraction within the total saturation.

A core flooding experiment was conducted using a composite core consisting of two plugs (CO2F1A and CO2F1B) from the Nini West Field to simulate reservoir conditions during CO_2 storage operations. The procedure involved sequential injection of formation brine and $scCO_2$ under reservoir temperature and pressure, mimicking the intermittent injection cycles expected during ship-based CO_2 transport and storage. Prior to flooding, the cores were aged with stock-tank oil at irreducible water saturation to replicate in-situ wettability conditions. The CO_2-flooded samples were later analysed to assess changes in hydrocarbon content and composition. A key motivation for comparing the hydrocarbon fractions in this sample to those in solvent-cleaned plugs was to investigate whether exposure to $scCO_2$ induces asphaltene precipitation within the rock matrix. By evaluating the enrichment or persistence of heavier hydrocarbon fractions, such as asphaltenes and solid bitumen, the analysis aims to determine the potential for in-situ precipitation caused by CO_2 injection.

The results show that the cores exhibited negligible saturations of mobile, semi-mobile, and immobile oil fractions. Notably, the solid bitumen/asphaltene content in this plug was comparable to that in solvent-cleaned core plugs, suggesting that asphaltene precipitation during $scCO_2$ flooding was either minimal or entirely absent. For a detailed procedure for the preparation and flooding of core CO2F1, we refer the reader to Andrianov et al. [44]. To facilitate comparison across samples, saturations were categorised into three groups: (1) movable oil saturation, comprising light and mobile oil fractions from both preserved and restored plugs; (2) non-movable oil saturation, encompassing immobile oil and solid bitumen/asphaltenes; and (3) semi-mobile oil saturation, maintained as a distinct category due to uncertainty about its precise contribution to overall oil mobility. The total oil saturations, along with their respective breakdowns, are summarised in Table 5 for both the preserved plugs and the restored plug REST1.

A particularly noteworthy trend emerges from this grouped analysis. Although the classification into movable, semi-mobile, and non-movable oil is based on inferred mobility rather than rheological behaviour, the measured non-movable oil saturations closely align with residual oil saturation (Sor) values reported in the literature. Specifically, the preserved core plugs exhibited non-movable saturations ranging from 8.8% to 14.3%, which falls within the 8–15% Sor range reported by

Table 5. Lumped saturation of the preserved and the restored samples

Sample type	Sample name	Total oil saturation (%)	Movable oil saturation (%)	Semi-movable oil saturation (%)	Non-movable oil saturation (%)
Preserved	PF1	39.4	14.1	10.7	14.3
	PF2	34.6	14.0	9.3	11.0
	PF3	48.5	14.4	19.7	14.2
	PB1	22.8	7.8	5.8	8.8
	PB2	38.1	11.6	12.6	13.7
	PB3	17.9	3.4	4.0	10.1
Restored	REST1	70.7	24.2	24.9	21.0

MacDonald and Mair (2003) [43] for the same reservoir. Similarly, the non-movable oil saturation of the restored plug REST1 aligns well with the residual saturation measured in plug CO2F1 (Sor = 19.7%) after undergoing water flooding but prior to CO_2 injection [44].

These findings suggest the potential of the ESH pyrolysis method as a rapid, practical tool for estimating residual oil saturation following water flooding. However, the method's reliability for this application remains to be fully validated, especially since ESH analyses have not yet been performed directly on water-flooded samples. Further experimental work is therefore recommended to confirm the method's applicability under these conditions

4 Conclusions

This study demonstrates the effectiveness and versatility of Extended Slow Heating (ESH) pyrolysis as a novel, rapid, and cost-efficient method for determining oil saturation, composition, and API gravity in reservoir samples. When applied to the depleted Nini West oil field, ESH provided oil saturation estimates from small ground rock samples that closely aligned with independently determined values. The method also enabled porosity correction by quantifying residual hydrocarbons left after core cleaning, thus improving the accuracy of petrophysical data. Beyond traditional core analysis workflows, ESH offers a high-resolution, low-sample-volume approach that can support enhanced reservoir characterisation and optimise strategies for CO_2 storage and enhanced oil recovery.

Experimental comparisons using preserved, brine-stored, cleaned, restored, and $scCO_2$-flooded core plugs revealed distinct trends in hydrocarbon mobility. Movable and semi-movable oils were largely displaced during brine storage, while immobile oil and solid bitumen/asphaltenes remained persistent. Anomalies, such as the lack of oil mobilisation in plug PB2, were attributed to incomplete brine immersion or positional effects within the core. The restored plug REST1 confirmed the method's validity, with ESH-estimated oil saturation (70.69%) matching the gravimetric reference (70%). Notably, REST1 exhibited elevated immobile oil saturation, likely due to ageing-induced wettability alteration. The $scCO_2$-flooded composite plug showed negligible movable oil and no significant asphaltene precipitation, underscoring ESH's ability to resolve changes in oil fractions caused by reservoir processes.

While ESH pyrolysis has demonstrated strong potential, its limitations must be considered. The technique relies on calibration with pure compounds, which may not fully reflect the complex behaviour of reservoir fluids. Nevertheless, ESH can be effectively integrated into both routine and special core analysis workflows as a complementary screening tool. It requires minimal procedural adaptation—mainly the inclusion of pyrolysis analysis on small samples—and can support sample selection, improve porosity correction. Future work should aim to understand the sensitivity of ESH saturation estimates to various parameters and uncertainties and explore broader applications across varied lithologies and reservoir types.

This research was conducted as part of Project Greensand Phase 2, an initiative focused on the safe and permanent storage of CO_2 within the depleted Nini West oil reservoir located in the Siri Canyon of the Danish North Sea. Project Greensand Phase 2 is a collaborative effort comprising a consortium of 23 Danish and international partners from both industry and academia, working collectively to advance carbon capture and storage (CCS) technologies. The project is generously supported by the Danish Energy Technology Development and Demonstration Programme (EUDP) under grant agreement #64021-9005, whose funding has been instrumental in enabling the scientific investigations and technological innovations presented in this study. The authors would also like to thank the reviewers, Yingxue Wang and Reza Askarinezhad, for their constructive comments, which have enhanced the clarity and quality of the manuscript.

References

1. J.M. Hunt, *Petroleum geochemistry and geology*, W.H. Freeman and Company, New York (1996), pp. 23–57.
2. H. Lee, K. Calvin, D. Dasgupta, G. Krinner, A. Mukherji, P. Thorne, C. Trisos, J. Romero, P. Aldunce, K. Barret, *Climate Change 2023: Synthesis Report, Summary for Policymakers*, IPCC, Intergovernmental Panel on Climate Change (IPCC) (2023).
3. M. Allen, O.P. Dube, W. Solecki, F. Aragón-Durand, W. Cramer, S. Humphreys, M. Kainuma, *Special Report: Global Warming of 1.5°C*, **677**, IPCC, Geneva, Switzerland (2018).
4. A. Raza, R. Gholami, R. Rezaee, V. Rasouli, M. Rabiei, *Significant aspects of carbon capture and storage – A review*, Petrol. **5**, 335–340 (2019). https://doi.org/10.1016/J.PETLM.2018.12.007
5. R.E. Hadlow, *Update of industry experience with CO_2 injection*, SPE Repr. Ser. **1999**, 24–29. https://doi.org/10.2118/24928-ms
6. R.J. Hwang, J. Ortiz, *Effect of CO_2 flood on geochemistry of McElroy oil*, Org. Geochem. **29**, 485–503 (1998). https://doi.org/10.1016/S0146-6380(98)00057-6
7. A.A. Bhatti, A. Raza, S.M. Mahmood, R. Gholami, *Assessing the application of miscible CO_2 flooding in oil reservoirs: a case study from Pakistan*, J. Pet. Explor. Prod. Technol. **9**, 685–701 (2018). https://doi.org/10.1007/S13202-018-0504-X
8. S. Thomas, *Enhanced oil recovery – An overview*, Oil Gas Sci. Technol. Rev. IFP **63**, 9–19 (2008). https://doi.org/10.2516/OGST:2007060
9. P.J. Jarboe, P.A. Candela, W. Zhu, A.J. Kaufman, *Extraction of hydrocarbons from high-maturity Marcellus Shale using supercritical carbon dioxide*, Energy Fuels **29**, 7897–7909 (2015). https://doi.org/10.1021/ACS.ENERGYFUELS.5B02059
10. S.B. Hawthorne, D.J. Miller, L. Jin, N.A. Azzolina, J.A. Hamling, C.D. Gorecki, *Lab and reservoir*

study of produced hydrocarbon molecular weight selectivity during CO_2 enhanced oil recovery, Energy Fuels **32**, 9070–9080 (2018). https://doi.org/10.1021/ACS.ENERGYFUELS.8B01645
11. K.J. Leontaritis, G. Ali Mansoori, *Asphaltene deposition: a survey of field experiences and research approaches*, J. Pet. Sci. Eng. **1**, 229–239 (1988). https://doi.org/10.1016/0920-4105(88)90013-7
12. M. Bonto, M.J. Welch, M. Lüthje, S.I. Andersen, M.J. Veshareh, F. Amour, A. Afrough, R. Mokhtari, M.R. Hajiabadi, M.R. Alizadeh, C.N. Larsen, H.M. Nick, *Challenges and enablers for large-scale CO_2 storage in chalk formations*, Earth Sci. Rev. **222**, 103826 (2021). https://doi.org/10.1016/J.EARSCIREV.2021.103826
13. H.I. Petersen, K.H. Blinkenberg, K. Anderskouv, A. Rudra, X. Zheng, H. Sanei, *Spatial distribution of remaining movable and non-movable oil fractions in a depleted Maastrichtian chalk reservoir, Danish North Sea: Implications for CO_2 storage*, Int. J. Coal Geol. **295**, 104624 (2024). https://doi.org/10.1016/j.coal.2024.104624
14. H.I. Petersen, W.F. Al-Masri, A. Rudra, S. Mohammadkhani, H. Sanei, *Movable and non-movable hydrocarbon fractions in an oil-depleted sandstone reservoir considered for CO_2 storage, Nini West Field, Danish North Sea*, Int. J. Coal Geol. **280**, 104399 (2023). https://doi.org/10.1016/J.COAL.2023.104399
15. R. Stenshøj, A. Abarghani, N. Badrouchi, Y. Yu, S.A. Smith, A. Rudra, H.I. Petersen, H. Sanei, *Hydrocarbon residue in a Danish chalk reservoir and its effects on CO_2 injectivity*, Mar. Pet. Geol. **156**, 106424 (2023). https://doi.org/10.1016/J.MARPETGEO.2023.106424
16. H. Sanei, J.M. Wood, O.H. Ardakani, C.R. Clarkson, C. Jiang, *Characterization of organic matter fractions in an unconventional tight gas siltstone reservoir*, Int. J. Coal Geol. **150–151**, 296–305 (2015). https://doi.org/10.1016/j.coal.2015.04.004
17. H. Sanei, *A method for estimating an amount of recoverable hydrocarbons in a rock sample*, Danish patent application **DK 2020 70146 A1**, (2021).
18. P. Jones, M.H. Tobey, *Pyrolytic oil-productivity index method for characterizing reservoir rock*, U.S. Patent **866,814**, 1999.
19. P. Jones, H. Halpern, M. Dahan, I. Bellaci, P. Neuman, R. Akkurt, S. Al-Qathami, M. Al-Amoudi, K. Malki, M. Dix, R. Zeriek, *Implementation of geochemical technology for real-time tar assessment and geosteering: Saudi Arabia*, (2007).
20. D. Kondla, H. Sanei, A. Embry, O.H. Ardakani, C.R. Clarkson, *Depositional environment and hydrocarbon potential of the Middle Triassic strata of the Sverdrup Basin, Canada*, Int. J. Coal Geol. **147–148**, 71–84 (2015). https://doi.org/10.1016/j.coal.2015.06.010
21. D. Kondla, H. Sanei, C.R. Clarkson, O.H. Ardakani, X. Wang, C. Jiang, *Effects of organic and mineral matter on reservoir quality in a Middle Triassic mudstone in the Canadian Arctic*, Int. J. Coal Geol. **153**, 112–126 (2016). https://doi.org/10.1016/j.coal.2015.11.012
22. O.H. Ardakani, H. Sanei, A. Ghanizadeh, D. Lavoie, Z. Chen, C.R. Clarkson, *Do all fractions of organic matter contribute equally in shale porosity? A case study from Upper Ordovician Utica Shale, southern Quebec, Canada*, Mar. Pet. Geol. **92**, 794–808 (2018). https://doi.org/10.1016/J.MARPETGEO.2017.12.009
23. S.B. Hawthorne, D.J. Miller, C.B. Grabanski, N. Azzolina, B.A. Kurz, O.H. Ardakani, S.A. Smith, H. Sanei, J.A. Sorensen, *Hydrocarbon recovery from Williston Basin shale and mudrock cores with supercritical CO_2: Part 1. Method validation and recoveries from cores collected across the basin*, Energy Fuels **33**, 6857–6866 (2019). https://doi.org/10.1021/acs.energyfuels.9b01177
24. S.B. Hawthorne, D.J. Miller, C.B. Grabanski, N. Azzolina, B.A. Kurz, O.H. Ardakani, S.A. Smith, H. Sanei, J.A. Sorensen, *Part 2. Mechanisms that control oil recovery rates and CO_2 permeation*, Energy Fuels **33**, 6857–6866 (2019). https://doi.org/10.1021/acs.energyfuels.9b01180
25. X. Dong, L. Shen, J. Zhao, et al., *A novel method to evaluate cleaning quality of oil in shale using pyrolysis pyrogram*, Energy Sci. Eng. **8**, 1693–1704 (2020). https://doi.org/10.1002/ese3.625
26. J. Sun, X. Dong, J. Wang, D.R. Schmitt, C. Xu, T. Mohammed, D. Chen, *Measurement of total porosity for gas shales by gas injection porosimetry (GIP) method*, Fuel **186**, 694–707 (2016). https://doi.org/10.1016/j.fuel.2016.09.010
27. B.A. Kurz, J.A. Sorensen, S.B. Hawthorne, S.A. Smith, H. Sanei, O. Ardakani, J. Walls, L. Jin, S.K. Butler, C.J. Beddoe, B.A.F. Mibeck (2018). The influence of organics on supercritical CO_2 migration in organic-rich shales. SPE/AAPG/SEG Unconventional Resources Technology Conference 2018, URTC 2018. https://doi.org/10.15530/URTEC-2018-2902743
28. C. McPhee, J. Reed, I. Zubizarreta, *Best practice in coring and core analysis*, Developments in Petroleum Science **64**, 1–15 (2015). https://doi.org/10.1016/B978-0-444-63533-4.00001-9
29. R.O. Baker, H.W. Yarranton, J.L. Jensen, *Conventional core analysis–rock properties*, (2015). https://doi.org/10.1016/B978-0-12-801811-8.00007-9
30. V. Tavakoli, *Geological core analysis: Application to reservoir characterization*, (2018).
31. Project Greensand Phase 1, EUDP, *Project Greensand Phase 1*, (accessed April 30, 2025). https://eudp.dk/en/node/16145
32. INEOS-Led Greesand to become the first full scale CO_2 storage facility in EU to help mitigate climate

change, *INEOS*, (accessed April 30, 2025). https://www.ineos.com/news/shared-news/ineos-led-greensand-to-become-the-first-full-scale-co2-storage-facility-in-eu-to-help-mitigate-climate-change/
33. L. Hamberg, G. Dam, C. Wilhelmson, T.G. Ottesen, *Paleocene deep-marine sandstone plays in the Siri Canyon, offshore Denmark–southern Norway*, Petroleum Geology Conference Proceedings **6**, 1185–1198 (2005). https://doi.org/10.1144/0061185
34. P. Schiøler, J. Andsbjerg, O.R. Clausen, G. Dam, K. Dybkjær, L. Hamberg, C. Heilmann-Clausen, E.P. Johannessen, L.E. Kristensen, I. Prince, J.A. Rasmussen, *Lithostratigraphy of the Palaeogene–Lower Neogene succession of the Danish North Sea*, GEUS Bull. **12**, 1–77 (2007). https://doi.org/10.34194/GEUSB.V12.5249
35. R. Weibel, H. Friis, A.M. Kazerouni, J.B. Svendsen, J. Stokkendal, M.L.K. Poulsen, *Development of early diagenetic silica and quartz morphologies - Examples from the Siri Canyon, Danish North Sea*, Sediment Geol. **228**, 151–170 (2010). https://doi.org/10.1016/j.sedgeo.2010.04.008
36. H.I. Petersen, N. Springer, R. Weibel, N.H. Schovsbo, *Sealing capability of the Eocene–Miocene Horda and Lark formations of the Nini West depleted oil field – implications for safe CO_2 storage in the North Sea*, Int. J. Greenhouse Gas Control **118**, 103675 (2022). https://doi.org/10.1016/J.IJGGC.2022.103675
37. O.B. Nielsen, E.S. Rasmussen, B.I. Thyberg, *Distribution of clay minerals in the Northern North Sea Basin during the Paleogene and Neogene: A result of source-area geology and sorting processes*, J. Sediment. Res. **85**, 562–581 (2015). https://doi.org/10.2110/JSR.2015.40
38. J.B. Svendsen, H.J. Hansen, T. Stærmose, M.K. Engkilde, *Sand remobilization and injection above an active salt diapir: The Tyr sand of the Nini Field, Eastern North Sea*, Basin Res. **22**, 548–561 (2010). https://doi.org/10.1111/J.1365-2117.2010.00480.X
39. The Danish Energy Agency, *Oil and Gas in Denmark 2013*, Copenhagen (2014).
40. N.H. Schovsbo, H.I. Petersen, R. Weibel, H.D. Holmslykke, N. Springer, *Characterising and evaluation of the seal capacity based on core and cutting analysis of the Nini-4 and Nini-4a wells. Project Greensand - WP4 final report*, Copenhagen: GEUS (2021). https://doi.org/10.22008/GPUB/34598
41. N. Keulen, R. Weibel, S.N. Malkki, *Mineral-specific Quantitative Element Mapping Applied to Visualization of Geochemical Variation in Glauconitic Clasts*, Front. Earth Sci. (Lausanne) **10**, 788781 (2022). https://doi.org/10.3389/FEART.2022.788781
42. R. Weibel, N. Keulen, M. Olivarius, S.N. Malkki, H.D. Holmslykke, S. Mohammadkhani, D. Olsen, N.H. Schovsbo, *Petrography and mineralogy of greensand in the Nini area including mineral reactions in CO_2 flooding experiments. Greensand Project Phase 1 WP2*, Copenhagen: GEUS (2021). https://doi.org/10.22008/GPUB/34600
43. I. MacDonald, K. Mair, *Dong E & P A / S Well: Nini-4 Well Number: 5605 / 10-4 Conventional Core Analysis Report Number: AF790*, Aberdeen (2003).
44. N. Andrianov, S. Mohammadkhani, B. Rostami, W.F. Al-Masri (2025). *Intermittent injection of supercritical CO_2 in oil–brine-saturated rocks: Experimental data and numerical modelling*. International Journal of Greenhouse Gas Control **144**, 104382. https://doi.org/10.1016/j.ijggc.2025.104382